

RSC Advances



This is an *Accepted Manuscript*, which has been through the Royal Society of Chemistry peer review process and has been accepted for publication.

Accepted Manuscripts are published online shortly after acceptance, before technical editing, formatting and proof reading. Using this free service, authors can make their results available to the community, in citable form, before we publish the edited article. This *Accepted Manuscript* will be replaced by the edited, formatted and paginated article as soon as this is available.

You can find more information about *Accepted Manuscripts* in the [Information for Authors](#).

Please note that technical editing may introduce minor changes to the text and/or graphics, which may alter content. The journal's standard [Terms & Conditions](#) and the [Ethical guidelines](#) still apply. In no event shall the Royal Society of Chemistry be held responsible for any errors or omissions in this *Accepted Manuscript* or any consequences arising from the use of any information it contains.

Phase formation and stability of alloy phases in free nanoparticles: some insights

Kirtiman Deo Malviya, Chandan Srivastava and K. Chattopadhyay

Department of Materials Engineering, Indian Institute of Science, Bangalore 560012

Corresponding author: K. Chattopadhyay,

Email: kamanio@materials.iisc.ernet.in

Telephone No.: 91 80 22932262; Fax: 918023600472

Abstract: This paper explores phase formation and phase stability in free nanoparticles of binary alloys. A procedure for estimating the size and composition dependent free energies incorporating the contributions from the interfaces have been presented. Both single phase solid solution and two phase morphology containing interphase interfaces have been considered. Free energy scenario has been evaluated for two binary alloy systems Ag–Ni and Ag–Cu to predict the microstructure of the alloy nanoparticles at different size ranges as a function of composition. Both Ag–Cu and Ag–Ni systems exhibit wide bulk immiscibility. Ag–Ni nanoparticles were synthesized using the wet chemical synthesis technique whereas Ag–Cu nanoparticles were synthesized using laser ablation of Ag–Cu target immersed in distilled water. Microstructural and compositional characterization of Ag–Ni and Ag–Cu nanoparticles on a single nanoparticle level was conducted using transmission electron microscopy. Nanoparticle microstructures observed from the microscopic investigation have been correlated with thermodynamic calculation results. It is shown that the observed two phase microstructure consisting of Ag–Ni solid solution in partial decomposed state coexisting with pure Ag phases in the case of Ag–Ni nanoparticles can be only be rationalized by invoking the tendency for phase separation of an initial solid solution with increase in nanoparticle size. Smaller sized Ag–Ni nanoparticles prefer a single phase solid solution microstructure. Due to increase in particles size during the synthesis process the initial solid solution decomposes into ultrafine scale phase separated microstructure. We have shown that it is necessary to invoke critical point phenomenon and wetting transition in systems showing critical point that lead to phase separated Ag–Ni nanoparticles providing catalytic substrate for the nucleation of equilibrium Ag over it. In the case of Ag–Cu system, we report the experimental observation of a core shell structure at small sizes. This can be rationalized in terms of a metastable solid solution. It is argued that the nucleation barrier can prevent the formation of

biphasic morphology with internal interface. In such a situation, demixing of the solid solution can bring the system to a lower energy configuration. This has led to the observed core-shell morphology in Ag-Cu system during room temperature synthesis.

Keywords: Nanoparticle, thermodynamics, phase stability, immiscible alloys, solid solution, size effect

1. Introduction

In recent years, studies on phase stability and phase transformations in nano-sized systems have gained considerable scientific and technological importance. These studies are needed to comprehend the fundamental science behind the phase stability criterion prevalent in systems at the nanometric length scale.¹⁻⁷ One interesting effect of the size induced alteration in bulk phase stability observed in the case of nano-sized isolated particles is the realization of miscibility leading to the formation of solid solution between immiscible component atoms.⁸⁻¹⁰ Elemental immiscibility at the bulk scale results from a large difference in the sizes of the component atoms and a positive enthalpy of their mixing.¹¹ Size-induced enhancement in miscibility is extremely relevant as it can facilitate manufacturing of novel alloys with exploitable technological properties.⁸ Although several experimental and theoretical studies on the phenomenon of size induced enhancement in miscibility have been reported by several research groups^{8,9,12}, many relevant issues related to the phase stability and microstructure still need to be addressed in a comprehensive manner. Furthermore, with respect to the understanding of the phase stability in systems with nanometric length scale, it should be emphasized that apart from the bulk-to-nano comparisons, the focus also should be on the “size effect” aspects. By “size-effect” it is meant that within the nano-scale regime, changes in the value of the surface and interface energies and the corresponding changes in the thermodynamic functions due to small changes in the size of the system is quite significant¹³⁻¹⁸.

Present work explores and extends some of our current ideas on the size effect in alloy particles at nanometric length scale. These include few critical results obtained recently that have the potential to throw light on the phase stability issues at small scale. In particular, in this paper we develop a general thermodynamic description of the alloys at small scale using the existing

knowledge of thermodynamics of pure element and extending them to the case of alloys. However, before one dwells into the issue of phase transition and stability at small scale, one needs to explore the kind of equilibrium that is expected at small scale for the case of alloys. Since phase transformation is a kinetic process involving mass transport, it is possible to describe equilibrium in terms of diffusion distance. In the case of bulk, the time required for the two phases to equilibrate their chemical potentials is generally large. The diffusion distance given by the expression D_{diff}/V where D_{diff} is the diffusivity and V is the growth velocity is much smaller than the dimension of each phase in equilibrium. In such a case, we adopt the concept of local equilibrium where only the composition of the phases at the phase interface is dictated by that given by the phase diagram. The diffusional mass flow in such a case occurs by the flow across the chemical potential gradient. The exceptions to this occur during nucleation process as well as in some instances during decomposition of metastable solid solution in an immiscible system when the transport process is dictated by fluctuation. In general, the time to reach global equilibrium is dictated by system size. In the case of liquid to solid transition, a growth rate of 10^{-2} m/sec and diffusivity of 10^{-8} m²/sec which is typical of such transition will yield a diffusion distance of 1 μm . Therefore, for any system size less than one micron, the liquid ahead of the growth interface will be globally mixed and hence full equilibrium can be assured. In the case of solid state, the growth rates are much smaller (of the order of $\mu\text{m/s}$). This often is countered by reduced diffusivity in solid state. The diffusion distance can still be $\sim 1 \mu\text{m}$ if the diffusivity is of the order 10^{-12} m²/s. For systems with sluggish diffusivity, this can be even smaller. In general, however, it is reasonable to expect full equilibrium in treating phase changes in nanoparticles. Thus, thermodynamics should reasonably accurately predict the co-existing phases and their transitions as a function of temperature for these particles. In developing an expression

for free energy changes for nanoparticles, one, however, needs to consider the surface and interface energies. In the following we first review the size dependent free energies of pure elements. Following this we shall attempt to develop an expression to estimate the free energies of alloy particles.

2. Size dependent surface energy of pure fcc elements

Thermodynamics at small size is dominated by the surface energy. However, the surface energy of small system is difficult to measure due to experimental constraints. Different methods are adopted by different research groups to estimate the surface energy of nanosize free particles. One of the methods is to find the vapor pressure difference due to change in particle size to get the surface energy of the pure elements. Piuz and Borel¹⁸ had calculated the surface energy of small crystals of pure Ag by calculating vapor pressure difference due to change in particle size. The surface energy is related to the chemical potential by the Gibbs Thomson's relation²⁰ given by

$$\mu = \mu_{\infty} + \frac{2\gamma}{\rho r} \quad \text{.....(1)}$$

In this expression, γ is the average surface energy of a spherical particle with radius r ; ρ is the specific mass and μ_{∞} is chemical potential in a crystal of infinite dimension. The well-known Kelvin equation²¹ can be obtained by equating the chemical potentials of crystal and the vapor and is given by

$$\ln \frac{p(r)}{p(\infty)} = \frac{2\gamma}{r\rho RT} \quad \text{.....(2)}$$

Where, $p(r)$ is the actual vapor pressure of particle size r and $p(\infty)$ is the saturated vapor pressure, R is gas constant and T is the temperature. Therefore in order to obtain surface energy

we need to know $p(r)$. This can be estimated from the change in size of the particle using Langmuir law¹⁹ given by,

$$\frac{dr}{dt} = \alpha p \left(\frac{M}{2\pi RT} \right)^{1/2} \dots\dots\dots(3)$$

Here, α is the evaporation coefficient, p is the actual vapor pressure of particle, M is the molar volume.

Piuz and Borel¹⁹ used this to obtain equilibrium surface energy. However, these experiments can also be used to determine size dependent surface energy. The size dependent surface energy can also be obtained by measuring the changes in the lattice parameter with size. This quantity with the knowledge of modulus and an isotropic assumption allow us to estimate pressure on the particles due to surface energy which with the help of Kelvin equation can yield an estimate of surface energy value.

Recently Liu et al.²² have developed methods of estimating the surface energy of small particles of pure elements using the size dependent cohesive energy of the pure metal. This is elaborated in a later section. The plot of size dependent surface energy of pure Ag and Ni estimated from this formalism is shown in Fig. 1. The figure indicates significant increase in surface energy at small sizes. The extrapolated surface energies of 1.25 J/m² and 2.45 J/m² matches well with the reported bulk surface energies²³ of Ag and Ni respectively. It should be noted that the thermodynamic calculations that produced the curve for variation in surface free energy with particle size in Fig. 1 considers average surface energy of a fcc crystal having equilibrium truncated octahedron geometry with clear crystal-air interfaces. In this study, since Ag-Ni and Ag-Cu nanoparticles grow in the liquid medium, the assumption may need modification. We have also ignored the effect of concentration gradient and hence contribution

of the gradient energy. The experimental results presented are a temporal snapshot during the growth. These are larger than the critical size for solid solution which the particles have evolved through at the initial stages. Since they are larger, the initial solid solution is expected to start decomposing in a spontaneous manner (possibly through spinodal decomposition). This is exactly what has been observed and indirectly support our model.

Surface energy plays a crucial role in phase formation at small scale. Although the surface energy contributions are generally neglected in the equilibrium phase diagram, it cannot be neglected at small sizes. The free energy function in this case should contain surface energy terms as contribution from surfaces and interfaces can be significant. For alloys, the geometry of the various surfaces needs to be known to estimate the surface energy contribution to the overall free energy. Fig. 2 shows two configurations of free nanoparticles that are possible in a particle of two components (A and B) at small length scale. The nanoparticles can be biphasic with an interphase interface separating them (Fig. 2a). The two elements A and B may also be completely mixed yielding nanoparticles of solid solution (Fig. 2b). In the following sections we present the free energy functions incorporating the size dependent free energies which can be used to estimate free energies of nanoparticles of different binary systems.

3. Free energy of biphasic free nanoparticles containing interphase interface

This corresponds to situation illustrated in Fig. 2a. Here each free nanoparticle contains two phases, A and B separated by an internal interphase interface. Each biphasic particles have three surface energy contributions. Two of them arise from free surfaces surrounding the two phases in the particle. The third arise from the interface between the two phases. Therefore, the free energy of such a free nanoparticle can be expressed as:

$$G_{biph} = x_A G_A + x_B G_B + \alpha_A S_A \gamma_A(D) + \alpha_B S_B \gamma_B(D) + G_{int}(D) \dots\dots\dots(5)$$

Where, x_A and x_B are the mole fractions of phase A and B respectively. G_A and G_B are molar free energies of phase A and phase B; $\gamma_A(D)$ and $\gamma_B(D)$ are the size dependent specific surface energy (surface energy per unit area) where D is the diameter of the particle; S_A and S_B are the surface areas occupied by one mole of A and B respectively; α_A and α_B are the ratios of atoms at the surface and in the bulk of A and B respectively. The last term $G_{\text{int}}(D)$ represents the interfacial energy between phase A and B. Considering the case when both A and B contain only one component, the surface energy can be calculated by the relation given by Turnbull²⁴. It consists of two terms, the geometrical term (γ_{geo}) and the chemical (γ_{chem}) term. Therefore $G_{\text{int}}(D)$ can be written as²⁵,

$$G_{\text{int}} = S_{\text{int}}(\gamma_{\text{geo}} + \gamma_{\text{chem}}) \quad \dots\dots\dots(6)$$

where, $\gamma_{\text{geo}} = [0.33(\gamma_A(D) + \gamma_B(D))] / 2 \quad \dots\dots\dots(7)$

and $\gamma_{\text{chem}} = \left\{ x_A \Delta H_{\text{BinA}} / [C_0 (V_A)^{2/3}] + x_B \Delta H_{\text{AinB}} / [C_0 (V_B)^{2/3}] \right\} \quad \dots\dots\dots(8)$

The term S_{int} is the interfacial area between A and B phases. ΔH_{AinB} (or ΔH_{BinA}) is the chemical interaction parameter for infinite dilution of A in B (or B in A). These quantities are available in the literature²⁶. The quantities V_A and V_B are the molar volumes of A and B respectively and C_0 is a constant generally taken as 4.5×10^8 [ref. 27].

4. The free energy of nanoparticles containing single phase solid solution of A and B

In the case described above, each phase contains only one component and there is no alloy formation between A and B except at the interface when the two pure phases interact. Fig. 2b describes the second scenario. Here both the components interact and form complete solid solution yielding a free single phase alloy particle. Here the surface energy of the alloy

nanoparticle depends on both size and the composition of the alloy. The free energy of solid solution (G_{ss}) in such a case is given by

$$G_{ss} = x_A G_A + x_B G_B + \Delta G_{mix} + (2\gamma_{ss}(D, x)V_{AB}) / (D / 2) \quad \dots\dots\dots(9)$$

Here, x_A and x_B are the mole fractions of phase A and B respectively, G_A and G_B are the molar free energies of A and B respectively, ΔG_{mix} is the excess free energy of the alloy and $\gamma_{ss}(D, x)$ is the size and composition dependent specific surface energy (surface energy per unit area) of the nanoparticle with solid solution between element A and B. The term V_{AB} represents the molar volume of solid solution and D is the diameter of the particle. Free energy of an alloy phase due to mixing (ΔG_{mix}) is given by,

$$\Delta G_{mix} = \Delta H_{mix} - T\Delta S_{mix} \quad \dots\dots\dots(10)$$

Where ΔH_{mix} and ΔS_{mix} are the enthalpy and entropy of mixing terms respectively. Assuming ideal solution, the entropy term can be written as

$$\Delta S_{mix} = -R[x_A \ln x_A + x_B \ln x_B] \quad \dots\dots\dots(11)$$

where R is the gas constant. According to Miedema model²⁸ the enthalpy of mixing (ΔH_{mix}) has three contributions, chemical (ΔH^{chem}), elastic (ΔH^{el}) and structural (ΔH^{str}) and can be expressed as

$$\Delta H_{mix} = \Delta H^{chem} + \Delta H^{el} + \Delta H^{str} \quad \dots\dots\dots(12)$$

The ΔH^{chem} term is related to electron distribution generated at the interface between dissimilar unit cells. This is expressed as²³,

$$\Delta H^{chem} = x_A x_B [x_A \Delta H_{BinA}^{chem} + x_B \Delta H_{AinB}^{chem}] \quad \dots\dots\dots(13)$$

Here ΔH_{AinB}^{chem} (ΔH_{BinA}^{chem}) is the chemical interaction parameter [25].

The elastic (ΔH^{el}) contribution to the enthalpy of mixing arises due to the atomic mismatch of element A and B and is given by²⁹,

$$\Delta H^{el} = x_A x_B [x_A \Delta H_{BinA}^{el} + x_B \Delta H_{AinB}^{el}] \quad \dots\dots\dots(14)$$

The term ΔH_{AinB}^{el} (or ΔH_{BinA}^{el}) represents the elastic interaction parameter and can be calculated by the following relation,

$$\Delta H_{BinA}^{el} = 2S'_A (V_B^* - V_A^*)^2 / (3V_A^* + 4S'_A k_B V_B^*) \quad \dots\dots\dots(15)$$

where S'_A & S'_B are the shear moduli; V_A^* and V_B^* are the effective molar volumes corrected for the charge transfer effects; k_A and k_B are the compressibility factors for of the elements A and B respectively.

The structural contribution (ΔH^{str}) [ref. 30] arises from the change in valence and crystal structure of the system and is given by,

$$\Delta H^{str} = E_{alloy}^{str} (Z_{alloy}) - [x_A E_A^{str} (Z_A) + x_B E_B^{str} (Z_B)] \quad \dots\dots\dots(16)$$

Here the Z_{alloy} , Z_A and Z_B are the average number of valence electrons per atom for the alloy, component A and component B respectively. The terms E_{alloy}^{str} , E_A^{str} , E_B^{str} are the lattice stability parameter of the alloy, A and B respectively. In order to estimate equation (6), we now need to know the surface energy which is both composition and size dependent.

Estimation of composition and size dependence of surface energies:

We have already briefly discussed the size dependence of surface energies. The specific surface energy $\gamma_{ss}(D, x)$ can be expressed in terms of surface energy per mole by the following expression³¹,

$$\gamma_{ss}(D, x) = N_i E_{surf}(D, x) / \pi \alpha N_A D^2 \quad \dots\dots\dots(17)$$

where, N_i is the number of atoms on the surface of a particle of diameter D , α is the shape factor and N_A is the Avogadro's number. The term $E_{surf}(D, x)$ is surface energy per mole. Liu and Jiang²² have presented a relation between $E_{surf}(D)$ and the cohesive energy $E_{coh}(D)$ for pure element. This is given as

$$E_{surf}(D) = k E_{coh}(D) \quad \dots\dots\dots(18)$$

Here, k is a function of coordination number of atoms at the surface and in the volume. Qi³² has extended the size dependence cohesive energy to incorporate the composition dependence in the case of solid solution containing two components A and B. This is given by the following expression

$$E_{coh}(D, x) = x_A E_A \left(1 - \frac{\alpha D^2}{n d_A^2} \right) + x_B E_B \left(1 - \frac{\alpha D^2}{n d_B^2} \right) \quad \dots\dots\dots(19)$$

Recently we have shown that this expression does not take into account interaction between two different atoms in the alloys²⁶. Incorporating this interaction the above expression can be modified as

$$E_c(D, x) = x_A E_A \left(1 - \frac{\alpha D^2}{n d_A^2} \right) + x_B E_B \left(1 - \frac{\alpha D^2}{n d_B^2} \right) - x_A x_B \Omega \quad \dots\dots\dots(20)$$

Where E_A and E_B are the bulk cohesive energy; d_A and d_B are the atomic diameter of element A and B respectively. α is the shape factor of the particle and n is the total number of atoms in particle size D . The interaction parameter is defined by Ω . Using the equations 20, 18 and 17, we can now calculate the composition and size dependence surface energies of solid solution. and hence can calculate the free energy change as a function of size and composition.

We now present the experimental results of our observations for two fcc based alloy systems, namely Ag-Ni and Ag-Cu system. The synthesis methods do influence the as synthesized phases. However, we shall strive to rationalize the observed results with regards to prevalent thermodynamic conditions which as we shall show, provide unique insights.

5. The case of Ag-Ni alloy nanoparticle

We now apply the above thermodynamic formulation to understand the phase formation and microstructure evolution in Ag-Ni alloy nanoparticles. Let us consider a nanoparticle of Ag-Ni solid solution. Fig. 3 gives the calculated free energy curve of Ag-Ni solid solution (G_{ss}) for a particles size of 7 nm. The hump in the free energy curve suggests that the solid solution if formed will tend to segregate compositionally without forming sharp interfaces. We have super imposed on this the free energy curve of two phase particles of fcc Ag and Ni of same size and containing interphase interface. As can be seen from these free energy curves, in this size range, the decomposition of the solid solution with the concomitant formation of interface between the phases will increase the free energy and hence will not be favorable. We shall now present the experimental results that we have obtained from chemically synthesized Ag-Ni alloy nanoparticles. The details are given elsewhere³¹. The goal is to attempt explaining the origin of the microstructure that has been observed in our experiments by considering the size dependent thermodynamics.

One of the striking results of our experiments is the formation of nanoparticles containing two phases. However, contrary to expectation, the two phases observed are equiatomic Ag-Ni solid solution and a pure Ag phase. A sharp interface separates these two phases. An example of this morphology is shown in Fig. 4 (a). As can be seen from this high resolution transmission electron microscope image of the particle, the solid solution phase has a size of ~6-7 nm and it

shares an interface with Ag phase. The decrease in lattice parameter of the solid solution phase as determined from the lattice fringe measurements clearly establish this phase to be a solid solution phase. Assuming that lattice parameters follow Vegard's law³³, the observed interplanar spacing of 0.220 nm for (111) planes represents the equiatomic composition of Ag and Ni. The lattice fringes from the other phase correspond to pure Ag. The size of this phase is much larger. A closer examination of the solid solution reveals distortions in the fringes suggesting the onset of process of demixing or compositional segregation through a probable spinodal like decomposition process. To illustrate the abundance of the particles with two phase microstructure, a low magnification bright field TEM image showing several of these particles and a selected area electron diffraction pattern (SAED), obtained from a group of these particles, showing diffraction signals corresponding to Ag-Ni solid solution phase and pure Ag phase is provided in the Fig. 4(b-c). In the SAED pattern, the ring with d-spacing of 0.24 nm corresponds to Ag-Ni solid solution phase and the ring with d-spacing of 0.22 nm corresponds to the pure Ag phase.

We propose that the present microstructure observation is a direct consequence of the phenomenon of critical point wetting. As shown by Cahn³⁴ and discussed recently by Puri *et al*³⁵ for the case of thin films, system with a miscibility gap containing critical point can undergo a wetting transition of one of the phases. As a consequence the surface of the phase (wetting phase) act as universally wetting surface and can wet any external surface. The consequence of this for the decomposition behavior of metallic glasses with miscibility gap has been discussed recently³⁶. We argue that these surfaces are ideal catalytic surface for heterogeneous nucleation and lead to a spontaneous nucleation of equilibrium phase in case of complete or even partial wetting³⁷.

In our earlier work³¹, detailed thermodynamic calculations including the energy of the surfaces of the nanoparticle and the interfaces between the two phases for a two phase existence within a nanoparticle indicates that there is a critical size when the free energy of the two pure phase separated by an interface within a particle and a particle of the same size where there is a complete solid solution is equal for a given overall composition. For sizes below that there is a driving force in favour of the formation of solid solution³¹. However, for the Ag-Ni system, the free energy curve representing solid solution is convex in nature as there is a positive heat of mixing for Ag and Ni. This indicates that even though the solid solution can form, it is not stable and is prone to solid state decomposition. In case the overall composition of the particle is not too near the bimodal line, the decomposition will most likely proceed through a spinodal decomposition triggered by a fluctuation process³⁸. The wave length of this fluctuation will depend on temperature and strain associated with the formation of solid solution³⁸. However, since it is a stochastic process, the probability of the initiation of the decomposition process will decrease with size. Thus, at a given temperature, fluctuations can be kinetically frozen below a certain size and one would expect to observe complete solid solution for very small sizes. However, as the particles grow, the solid state decomposition will set in. To understand the microstructure of the particles observed by us, we need to invoke at this stage another phenomenon associated with the spinodal decomposition known as critical point wetting^{34,35}. As mentioned earlier, during spinodal decomposition, one of the decomposing surfaces acquires the property of completely wetting any surfaces in contact with it. Thus one expects spontaneous nucleation of Ag (or Ni) on the surface of solid solution. In the present study, Ag-Ni nanoparticles were prepared by the chemical synthesis technique which is a bottom up approach for producing nanoparticles³¹. Therefore it should be emphasized that the particles nucleated and

grew from zero size to a finite size. Mechanistically, all the particles in the reaction mixture must have possessed a solid solution microstructure till the point at which some of them continued to grow over the critical size required for spinodals decomposition. Recent work³¹ provides the evidence for single phase solid solution structure for nanoparticles with sizes less than a critical size for the observation of spinodal decomposition. Once spinodal decomposition occurs in larger particles, critical point wetting will ensure the formation of terminal phase on the surface of solid solution phase. Thus the further growth of the particles will occur only by the growth of pure Ag leading to the observed morphology. A schematic illustrating the above described mechanism is provided in Fig. 5.

It should be noted that the size dependent thermodynamic arguments can be used for system sizes within the nanoscale regimen where the surface energy varies significantly with size. The stabilization of the solid solution in immiscible system is clearly a size dependent effect. However, the critical point wetting phenomenon is an universal phenomena that happens in system having critical point and undergoing the decomposition process. As the particles grow, the stabilization of the solid solution vanishes and the system enters phase separating regime. The critical point wetting phenomenon where one of the separating phase behaves as universal wetting surface occurs at this stage and the nucleation barrier on this surface vanishes. Thus pure silver which has lowest free energy forms spontaneously on this surface leading to the observed two-phase nanoparticle microstructure.

6. Microstructure evolution of alloy nanoparticles in Ag-Cu system by laser ablation

We now consider the case of Ag-Cu alloy nanoparticles. The synthesis in this case was carried out by laser ablation process under water. As a consequence, there exist important differences in the growth behavior compared to the case of Ag-Ni alloy. In general the particles

form rapidly during laser pulsing and get isolated by the surrounding fluid. The subsequent growth of the particles generally occurs by coalescence and not by diffusion of the solutes through the media. This is unlike the chemical process where the atoms can arrive over a period of time leading to a time dependent growth. In Fig. 6, we have presented the free energy curve at room temperature for three different sizes of Ag-Cu alloy particles namely 5 nm, 13 nm and 25 nm. Again we have considered the two cases as illustrated in Fig. 2. Since the heat of mixing is also positive in this case, the free energy curves for Ag-Cu solid solution exhibit a hump similar to Ag-Ni system. This indicates that the solid solution will have demixing tendency. The free energy curves of nanoparticles containing two phase (Ag and Cu) separated by an interface do not show this behavior.

An analysis of the free energy curves again allow us to arrive at some striking conclusions. Let us consider the free energy curve of 5 nm particles (Fig. 6a). It suggests that single phase particle containing solid solution is favorable in comparison to a two phase particle containing pure silver and copper. However, the solid solution will tend to demix and yield compositional segregation without creating an interface. The appearance of internal interface will raise the free energy. We note that we have not completely accounted for elastic energy in our calculation which may further stabilize the solid solution and reduce the miscibility gap. The above discussions yield following conclusions. Below a critical size, the nanoparticles of Ag-Cu alloy will form solid solution. A two phase equilibrium structure is not stable at these sizes. The solid solution can demix through segregation. However, solid solution will not decompose into two phase with an interface separating them.

For a 13 nm particle, the free energy curve of biphasic particles of Ag and Cu touches the free energy curve of solid solution at close to equiatomic composition (Ag₅₀ Cu₅₀) alloy (Fig.

6b). Fig. 6c shows the free energy situation for a 25 nm particle. An analysis of this and other curves with similar sizes in this range suggest that for a range of composition, solid solution can only exist as a metastable phase. A driving force exist for it to decompose into two phase with internal interface separating them. However, if it under goes demixing, it can again enter into a stable state in comparison to a state containing two distinct phases.

Let us examine the experimental results in the context of this analysis. Fig. 7a shows two laser ablated Ag-Cu alloy nanoparticles of ~25 nm and ~35 nm sizes respectively. No internal interface could be observed in both the particles. These are nanoparticles containing single phase Ag-Cu solid solution. The composition profile obtained using 1 nm beam in scanning transmission electron microscopy (STEM) mode using a TECHNAI F30 microscope is shown in Fig. 7b. We have presented the intensities of the signals originating from Ag and Cu. Clearly copper has segregated at the interface while the core is Ag rich. Fig. 7c shows quantification of the composition profile for the 25 nm particle. The nature of segregation of solid solution is clearly revealed. For comparison, we have presented a particle of similar size (Fig. 8) which was heated in an image furnace for 3 minutes at 650 °C. The microstructure reveals internal interface between the two phases. Composition profile (Fig. 8b) clearly identifies the particle to be biphasic containing copper rich and Ag rich phases. The free energy curves for the nanoparticles of Ag-Cu alloy at 650 °C are presented in Fig. 8c. Clearly the driving force for the formation of two phases with interphase interface is much larger at this temperature and hence the solid solution decomposes into biphasic particle.

For the un-annealed Ag-Cu nanoparticles, presence of Cu on the surface of the particles as shown by Fig. 7 can be justified from taking into consideration the combined effect of the critical point wetting phenomenon and relative ablations rates for Ag and Cu atoms from the Ag-

Cu target during the laser ablation reaction. As described earlier for the Ag-Ni case, with increase in the size of the Ag-Cu nanoparticles during ablation, initially formed Ag-Cu solid solution phase would undergoes spinodal decomposition at some critical particle size. This decomposition produces relatively Ag-rich and Cu-rich compositional waves in the particles. One such particle with compositional wave is shown in Fig. 9. Fig. 9(a) shows a high magnification TEM image of a Ag-Cu nanoparticle. Fig. 9(b) shows a Fast Fourier Transform (FFT) obtained from the image of the particles in Fig. 9(a). The FFT reveals the presence of rings corresponding to the planes with interplanar spacing values of 0.21 nm, 0.22 nm and 0.23 nm. When compared to the interplanar spacing values for different planes in the crystal of pure Ag and Cu phases, the observed d-spacing values denote the presence of solid solution phases with Ag-rich and Cu-rich compositions within the particle. An Inverse Fast Fourier Transform images (IFFT) derived from the rings with interplanar spacing values of 0.22 nm and 0.23 nm shown in Fig. 9 (c) and 9 (d) respectively reveal intermixed Ag-rich and Ni-rich compositional waves characteristic of a spinodically decomposed microstructure. It is well known that the ablation rate for pure metals is directly proportional to their atomic number³⁹. This signifies that Ag should have a higher ablation rate as compared to Cu. During the laser ablation experiment, the target therefore gets richer in Cu with time. A relatively Cu-rich target would produce relatively Cu-rich atomic flux at the later stages of the ablation process producing compositionally graded microstructure with increasing Cu concentration towards the surface of particles as seen in the present case (Fig. 7). As the target becomes Cu rich with the progress of ablation process, the atomic flux would be copper rich. Due to the zero undercooling that is required for spontaneous nucleation on the perfectly wettable surface provided by the

spinodically decomposed Ag-Cu particles (Fig. 9) due to critical point wetting and subsequent wetting transition³⁴ Cu atoms nucleate to produce a Cu rich surface.

7. Conclusions

We have presented a procedure for the estimation of size and composition dependent free energy function of fcc based metallic alloys taking into consideration biphasic alloy nanoparticles as well as nanoparticles of single phase solid solution. These free energy curves allow us to examine the possible phase evolution at different sizes. We show that it is possible to have solid solution at small sizes for alloys with high positive heat of mixing with extensive segregation. We note that wetting transition during spinodal decomposition can lead to a two phase structure of pure component and segregated solid solution. The experimental evidence of such occurrence has been presented for chemically synthesized Ag-Ni nanoparticles. For Ag-Cu alloy particle, the segregation can stabilize the alloy nanoparticles and the evidence of the formation of a segregated core shell like Ag-Cu solid solution particle is presented. These particles at higher temperature revert back to biphasic nanoparticles.

Acknowledgement

The authors would like to acknowledge the microscopy facilities available at Advanced Facility for Microscopy and Microanalysis (AFMM), The Indian Institute of Science, Bangalore, India. The funding from SERB and Department of Science and Technology, Government of India is gratefully acknowledged.

References

- 1 A.S. Shirinyan, A.M. Gusak, M. Wautelet, *Acta Materialia*, 2005, **53**, 5025-32.
- 2 M. Wautelet, A.S. Shirinyan, *Pure Appl. Chem.*, 2009, **81**, 1921-1930.
- 3 L.D. Gelb, K.E. Gubbins, R. Radhakrishnan, M.S. Bartkowiak, *Rep. Prog. Phys.*, 1999, **62**, 1573-1659.
- 4 S. Xiong, W. Qi, B. Huang, M. Wang, Y. Cheng, Y. Li, *J. Comput. Theor. Nanos.*, 2011, **8**, 2477-2481.
- 5 A.S. Shirinyan, M. Wautelet, *Nanotechnology*, 2004, **15**, 1720-1731.
- 6 F. Baletto, R. Ferrando, *Rev. Mod. Phys.*, 2005, **77**, 371-423.
- 7 M. Einax, W. Dieterich, and P. Maass, *Rev. Mod. Phys.*, 2013, **85**, 921-939.
- 8 P. Ayyub, *Int. J. Nanotechnol.*, 2009, **6**, 530-40.
- 9 Z. Zhang, T.M. Nenoff, J.Y. Huang, D.T. Berry, P.P. Provencio, *J. Phys. Chem. C*, 2009, **113**, 1155-1159.
- 10 K. D. Malviya and K. Chattopadhyay, *J. Phys. Chem. C*, 2014, **118**, 13228–13237
- 11 R. Najafabadi, D.J. Srolovitz, E. Ma, M. Atzmon, *J. Appl. Phys.*, 1993, **74**, 3144-3149.
- 12 S. Xiao, W. Hu, W. Luo, Y. Wu, X. Li, H. Deng, *Eur Phys J. B*, 2006, **54**, 479-84.
- 13 P. Buffat, J.P. Borel, *Phys. Rev. A*, 1976, **13**, 2287-2298.
- 14 P.R. Couchman, W.A. Jesser, *Nature*, 1977, **269**, 481-483.
- 15 M.O. Robbins, G.S. Grest, K. Kremer, *Phys. Rev. B*, 1990, **42**, 5579-5585.
- 16 L.H. Liang, D. Liu, Q. Jiang, *Nanotechnology*, 2003, **14**, 438-442.

- 17 K.K. Nanda, S.N. Sahu, S.N. Behera, *Phys. Rev. A*, 2002, **66**, 013208 (1-8).
- 18 C.Q. Sun, B.K. Tay, X.T. Zeng, S. Li, T.P. Chen, J. Zhou, H. L. Bai, E.Y. Jiang, *J. Phys.: Condens. Matter*, 2002, **14**, 7781-7795.
- 19 F. Piuz, J.P. Borel, *physica status solidi (a)*, 1972, **14**, 129-133.
- 20 R. Defay, I. Prigogine, A. Bellemans, D.H. Everett, *London: Longmans*, 1966.
- 21 W.L.X. Thomson, *Philosophical Magazine Series 4*, 1871, **42**, 448-452.
- 22 D. Liu, Q. Jiang, *Nanoelectronics Conference*, 2008 INEC 2008 2nd IEEE International 2008, p. 30-32.
- 23 A.R. Miedema, *Zeitschrift fuer Metallkunde/Materials Research and Advanced Techniques*, 1978, **69**, 6.
- 24 D. Turnbull, *Metals Park, Ohio: American Society of Metals*, 1955, 121-144.
- 25 X.Y. Li, Z.F. Li, B.X. Liu, *J. Alloys Compd.*, 2002, **334**, 167-172.
- 26 A.K. Niessen, F.R. de Boer, R. Boom, P.F. de Châtel, W.C.M. Mattens, A.R. Miedema *Calphad*, 1983, **7**, 51-70.
- 27 A.R. Miedema, *Z Metallkd.*, 1978, **69**, 287-292.
- 28 F.R. de Boer RB, W.C.M. Mattens, A.R. Miedema, A.K. Niessen, *Transition Metal Alloys* Amsterdam: North Holland; 1988.
- 29 J.D. Eshelby, New York: Academic Press; 1956.
- 30 L.J. Gallego, J.A. Somoza, J. A. Alonso, *Physica B: Condensed Matter*, 1989, **160**, 108-112.

- 31 C. Srivastava, S. Chithra, K.D. Malviya, S.K. Sinha, K. Chattopadhyay, *Acta Mater.*, 2011, **59**, 6501-6509.
- 32 W.H. Qi, *J. Mater. Sci.*, 2006, **41**, 5679-5681.
- 33 A.R. Denton, N.W. Ashcroft, *Phys. Rev. A*, 1991, **43**, 3161-3164.
- 34 J.W. Cahn, *J. Chem. Phys.*, 1977, **66**, 3667-3672.
- 35 K. Binder, S. Puri, S. Das, J. Horbach, *J. Stat. Phys.*, 2010, **138**, 51-84.
- 36 B.J. Park, H.J. Chang, D.H. Kim, W.T. Kim, K. Chattopadhyay, T.A. Abinandanan, S. Bhattacharaya. *Phys. Rev. Lett.*, 2006, **96**, 245503 (1-4).
- 37 H.B.W. Biloni, In: *Cahn RW HP, editor. Physical Metallurgy. 4 ed. Amsterdam: North-Holland*, 1996, p. 669-842.
- 38 D.A. Porter, K.E. Easterling, M.Y. Sherif. *Phase Transformations in Metals and Alloys: Taylor & Francis Group*, 2009.
- 39 R.A. Burdt, S. Yuspeh, K.L. Sequoia, Y. Tao, M.S. Tillack, F. Najmabadi, *J. Appl. Phys.*, 2009, **106**, 033310(1-5).

Figure Captions

Figure 1. Plot showing the calculated size dependent specific energy of (a) pure Ag and (b) pure Ni.

Figure 2. Schematic of the two distinct morphologies that can be observed in binary alloys: (a) biphasic nanoparticle with internal interface, (b) nanoparticle of single phase solid solution between elements A and B.

Figure 3. Calculated free energy curves for 7nm Ag-Ni alloy nanoparticle showing free energy curves for single phase solid solution (G_{ss}) and nanoparticle containing two phases (G_{biph}).

Figure 4.(a) A high resolution Transmission electron microscopy (TEM) micrograph of nanoparticle of Ag-Ni alloy obtained by chemical synthesis. The two phase particle consists of equiatomic Ag-Ni solid solution of diameter ~6-7nm surrounded by a pure Ag phase with sharp interface between the two phases (b)selected area electron diffraction pattern obtained from a group of two phase microstructured particles (c) TEM bright field image of two phase microstructured particles.

Figure 5. A schematic illustrating the possible mechanism of formation of two phase microstructure particles. The schematic shows a sequence where a small sized particle with a solid solution structure grows above a critical size which causes the solid solution phase to spinodally decompose into Ag-rich and Ni-rich phases. Subsequent to the spinodal

decomposition reaction, the Ag-rich phase provides a universal wetting surface for the pure Ag phase to nucleates and grows over it accordance with the critical point wetting phenomenon

Figure 6 Plots showing calculated free energy curves G_{ss} and G_{biph} for Ag-Cu alloy nanoparticles at room temperature for three different size of particles: **(a)** 5nm, **(b)** 13nm, **(c)** 25nm.

Figure 7(a) A STEM image of Ag-Cu alloy particles of size 35nm and 20nm, **(b)** distribution of intensity of Ag and Cu signals from EDS along the line as shown in (a), **(c)** composition distribution in the small Particle (25nm). Note the copper segregation at the outer shell and composition modulation of the solid solution near the core.

Figure 8(a) STEM image of Ag-Cu nano particle (~ 25 nm) similar to that shown in fig. 7 after heat treatment at 650°C for three minutes in a gold image furnace, **(b)** composition distribution of Ag and Cu along the arrowed line obtained by STEM analysis using a 1nm probe, **(c)** the free energy curve of G_{ss} and G_{biph} for the particle of the same size (25nm) at 650°C.

Figure 9(a) High magnification image of a nanoparticle **(b)** FFT image obtained from the particle in figure **(a)**, **(c)** Inverse Fourier Transform image of the regions in the particle corresponding to the phase represented by the ring with interplanar spacing value of 0.23 nm in the FFT **(d)** Inverse Fourier Transform image of the regions in the particle corresponding to the phase represented by the ring with interplanar spacing value of 0.22 nm in the FFT.

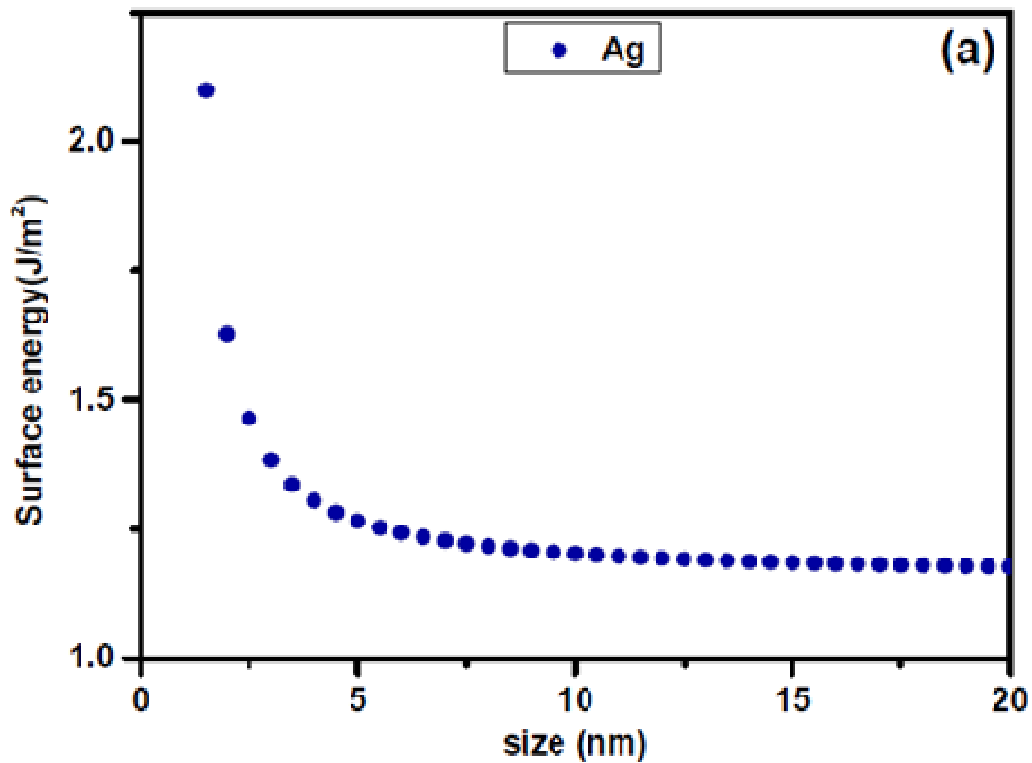


Fig 1(a)

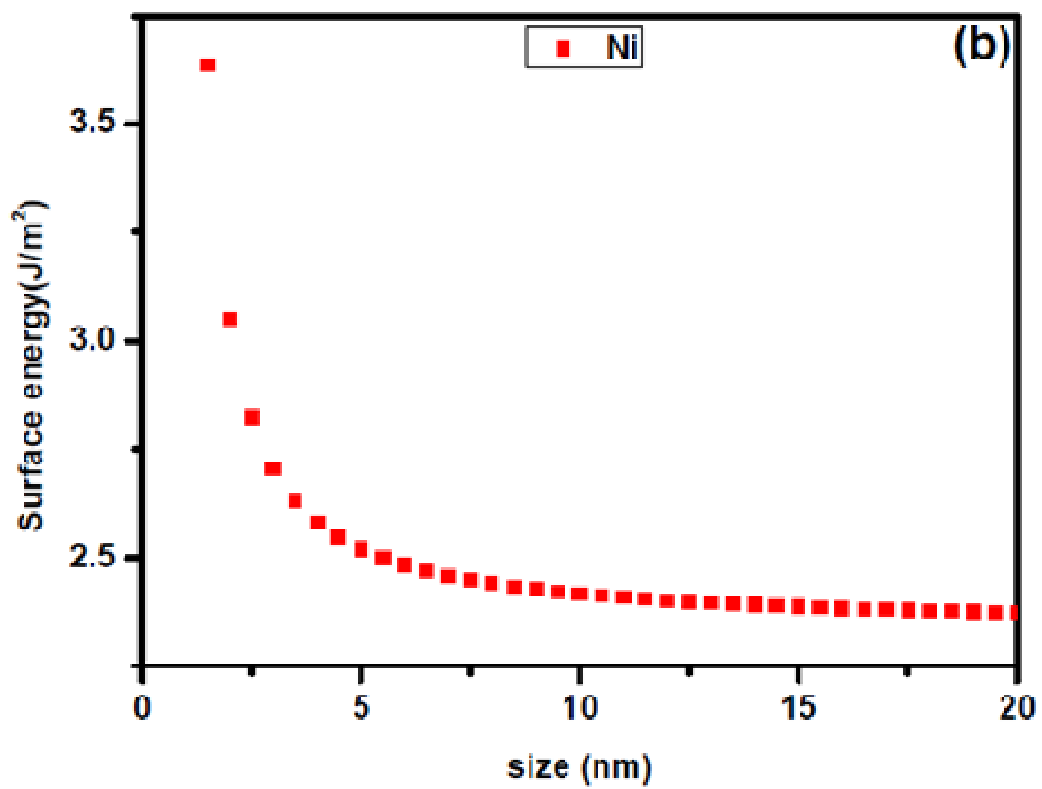
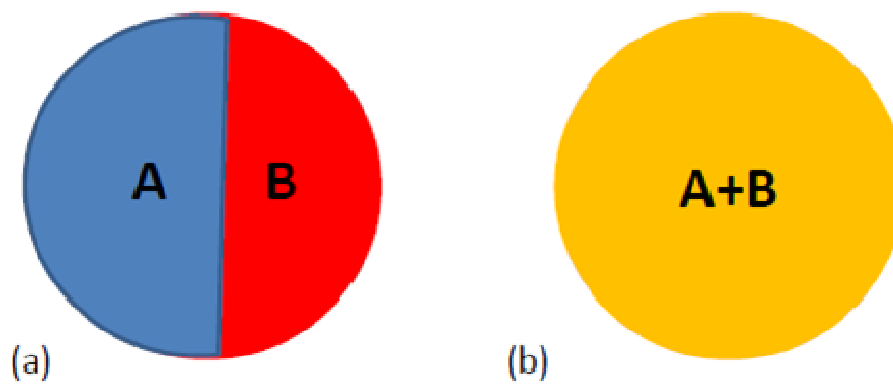
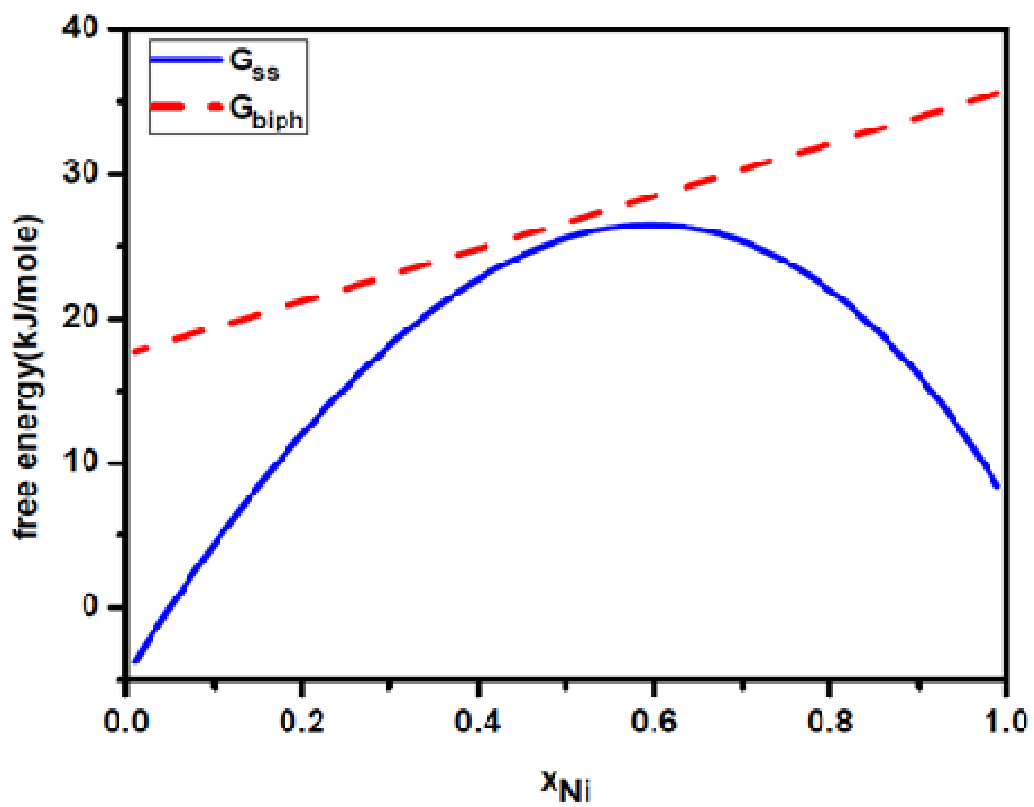
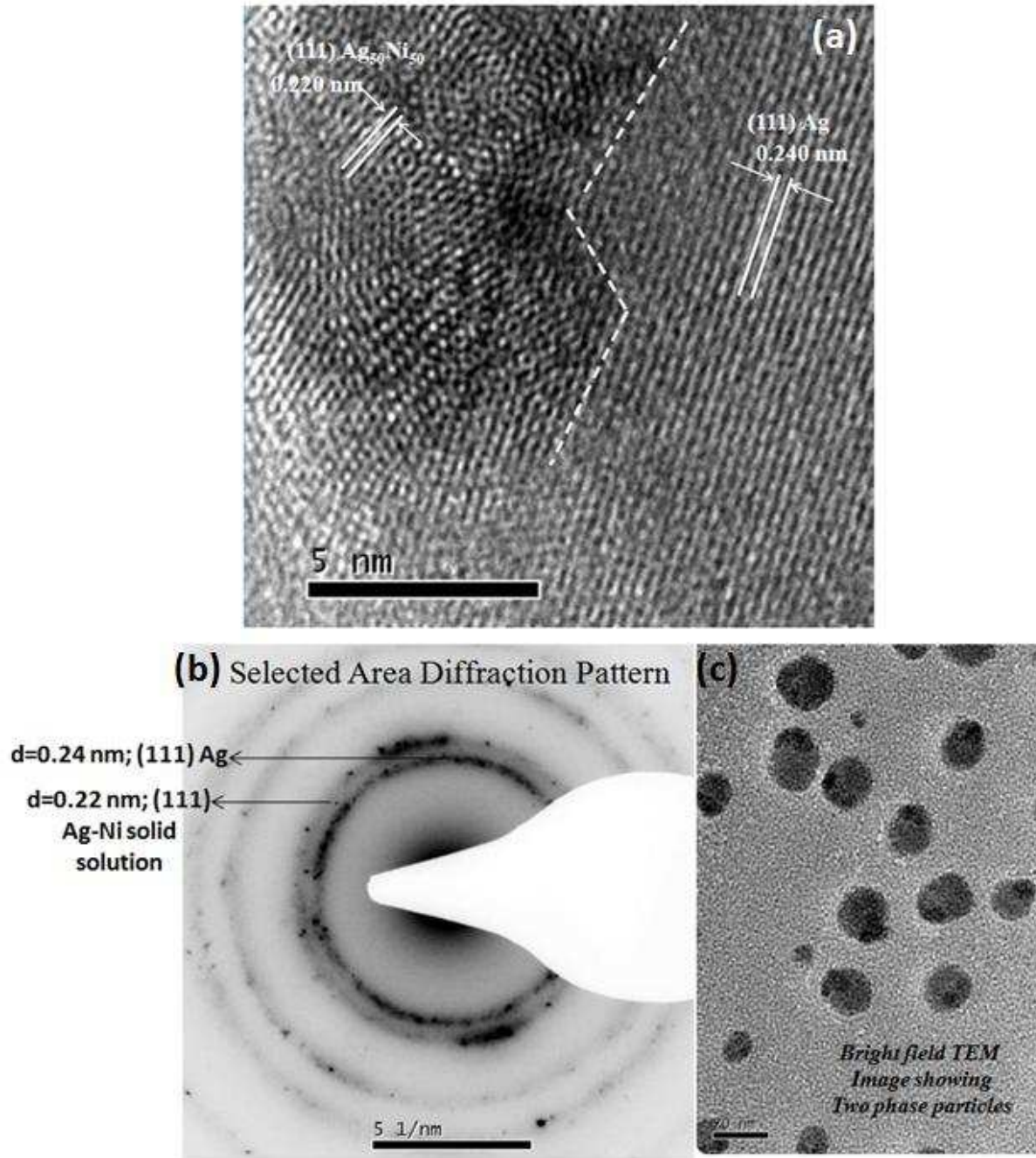
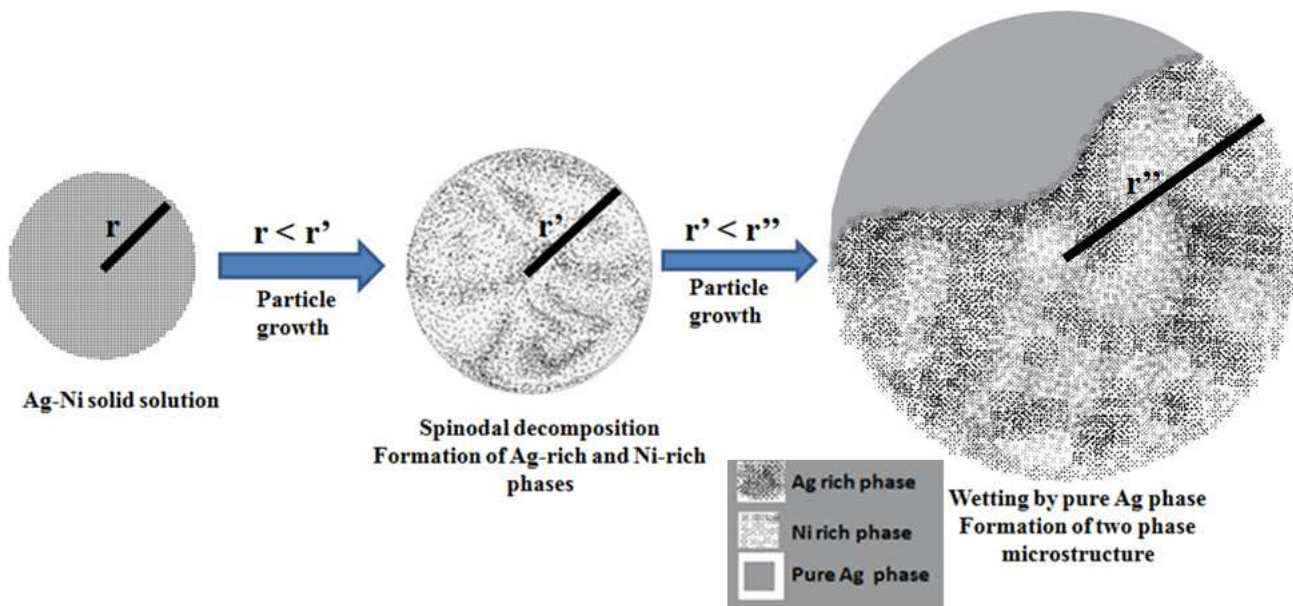
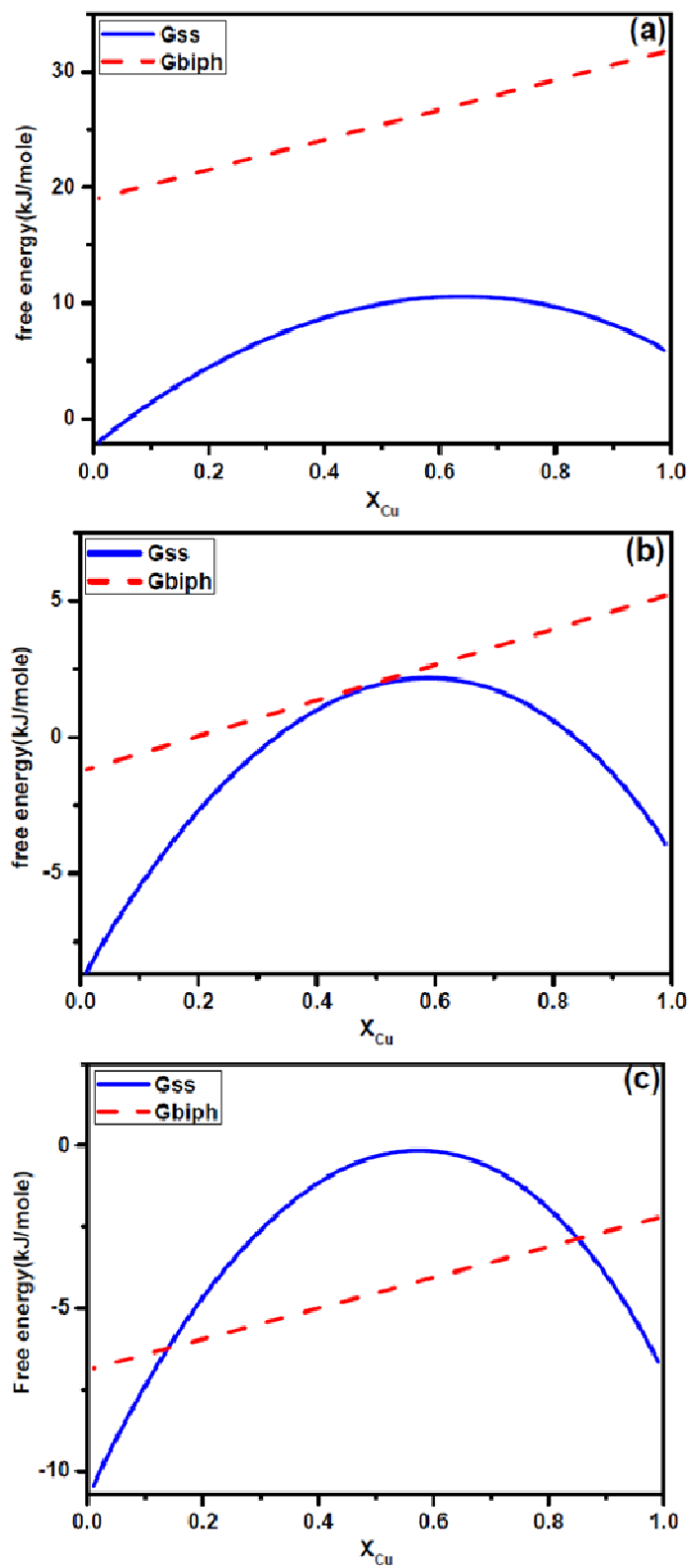


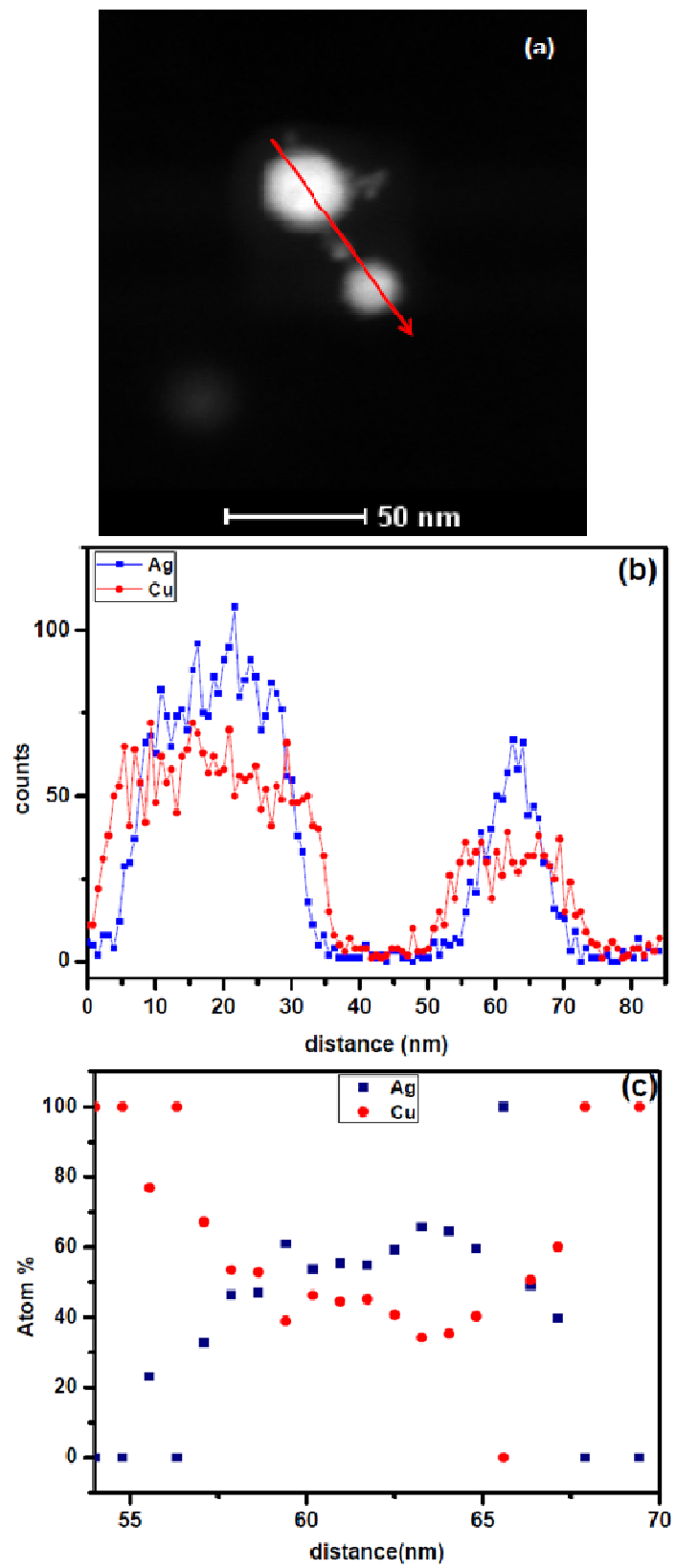
Fig 1(b)

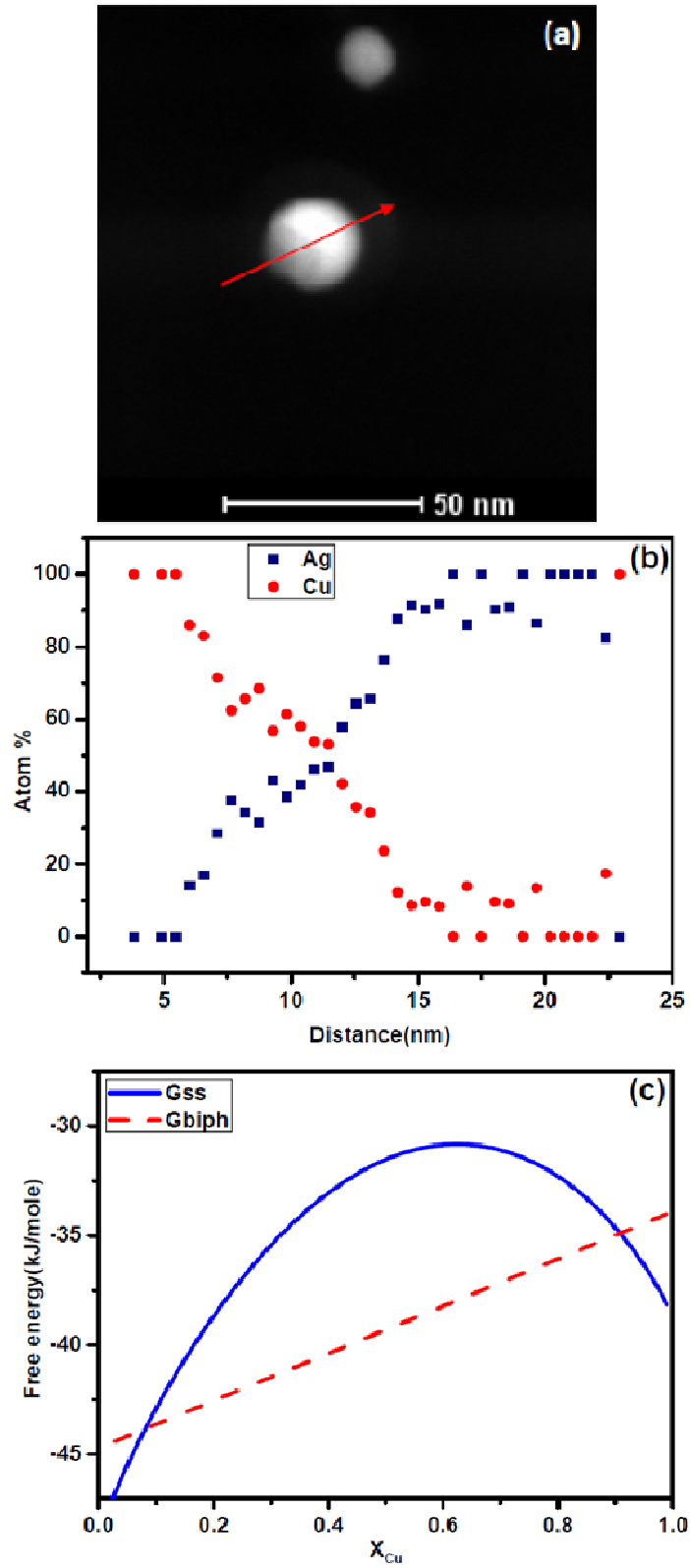
**Fig 2****Fig 3**

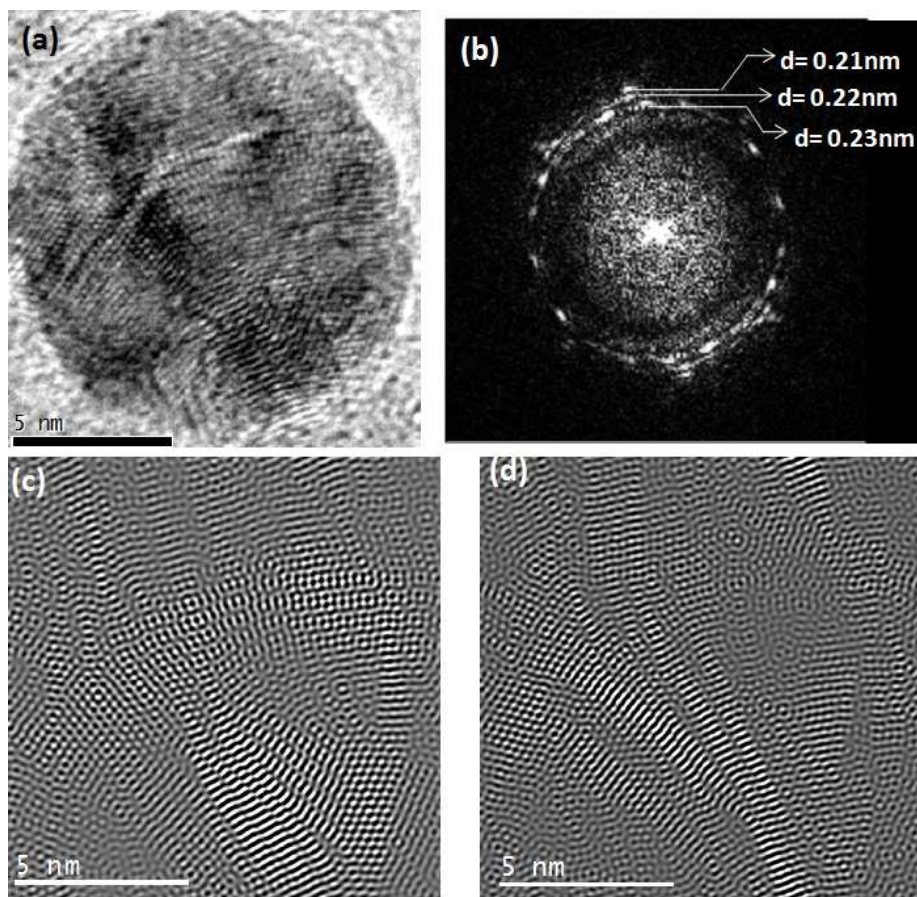
**Fig 4**

**Fig 5**

**Fig 6**

**Fig 7**

**Fig 8**

**Fig 9**